

Non-chaotic dynamics for Yang-Baxter deformed $AdS_4 \times CP^3$ superstrings

Jitendra Pal*, Hemant Rathi† and Dibakar Roychowdhury‡

Department of Physics, Indian Institute of Technology Roorkee, Roorkee
247667 Uttarakhand, India

Abstract

We explore a novel class of Yang-Baxter (YB) deformed $AdS_4 \times CP^3$ backgrounds which exhibit a non-chaotic dynamics for (super)strings those are propagating over it. We probe the classical phase space of these (semi)classical strings and calculate various chaos indicators. These include studying the Poincare sections and estimating the Lyapunov exponents which confirm an integrable phase space dynamics in the (semi)classical limit.

1 Introduction and summary

Understanding the chaotic behaviour [1]-[14] and the associated integrable structure in various examples of gauge/gravity correspondence [15]-[16] has been an outstanding problem for past couple of decades. While in most of these cases, one encounters a chaotic motion, there are some handful of examples those confirm non-chaotic dynamics and thereby an integrable structure.

Non-chaotic dynamics are therefore always special in holography. The central idea behind these analyses is to probe the classical phase space configuration of (semi)classical strings with various chaos indicators. These indicators ensure whether the phase space allows a KAM tori and thereby (quasi)periodic orbits [1]-[3]. Identification of these orbits in the first place, is the key step towards unveiling an integrable structure associated with the classical phase space.

Following the holographic duality [15]-[16], one can argue that these semiclassical strings are dual to a class of single trace operators in the large N limit of the dual QFT. This would therefore enable us to conjecture about the integrability of the dual QFT at strong coupling.

The purpose of the present paper is to apply these concepts to a novel class of Yang-Baxter (YB) deformed [17]-[28] backgrounds those were obtained until recently by the authors in [29]-[32]. These are the deformations of the original $AdS_4 \times CP^3$ background [33] where the deformation is generated through classical r - matrices satisfying the YB equation. However, unlike the undeformed case [34], the integrable structure of these deformed class of backgrounds are yet to be confirmed. We perform a systematic analysis to fill up this gap in the literature.

YB deformations, those were originally introduced as an integrable deformation of the sigma model [17]-[18], are based on the notion of classical r - matrices those satisfy YB equations. These r - matrices could be categorized into two classes. One of them satisfy modified classical Yang-Baxter equation (mCYBE) while the other classical Yang-Baxter equation (CYBE).

*jpal1@ph.iitr.ac.in

†hrathi@ph.iitr.ac.in

‡dibakar.roychowdhury@ph.iitr.ac.in

Classical r -matrices satisfying mCYBE have been applied to symmetric cosets [19] as well as $AdS_5 \times S^5$ super-cosets [20]-[22]. For the later case, the type IIB equations were confirmed until recently [24]. On the other hand, abelian r -matrices satisfying CYBE were applied to $AdS_5 \times S^5$ sigma models in [25] which were further generalized for the non-abelian case in [26]. For classical r -matrices satisfying CYBE, the resulting background is found to satisfy type IIB supergravity equations of motion [27]-[28].

Motivated by these $AdS_5 \times S^5$ examples, abelian r -matrices satisfying CYBE have been applied to $AdS_4 \times CP^3$ sigma models until very recently [29]-[32]. In their construction, the authors consider various YB deformations of the AdS_4 subspaces as well as the internal CP^3 manifold. These result into a class of deformed ABJM models which we summarise below.

Depending on the type of YB deformations, one eventually generates a class of gravity duals¹ [29]-[32] for (1) β deformed ABJM, (2) Noncommutative ABJM, (3) Dipole deformed ABJM and (4) Nonrelativistic ABJM. In the present paper, we consider (semi)classical string dynamics for each of these deformed backgrounds and calculate their respective chaos indicators.

The organization for the rest of the paper is as follows. In Section 2, we present the basic algorithm that has been followed in the paper. In Section 3, we apply this algorithm to each of the four examples of deformed ABJM those are listed above. Finally, we conclude in Section 4.

2 The algorithm

In the present work, we focus on two chaos indicators namely, the Poincare section and the Lyapunov exponent [1]-[3]. For the familiarity of the reader, below we briefly elaborate on them and outline basic steps to calculate these entities in a holographic setup.

The signatures of integrability or non-integrability can be differentiated by looking into the phase space dynamics of the system. Integrable systems do not exhibit chaos and the trajectories are (quasi)periodic at equilibrium points. Non-integrable systems, on the other hand, are associated with the phase space that could be mixed showing (quasi)periodic orbits for some initial conditions and chaotic for others.

For a $2N$ dimensional integrable phase space, there are N conserved charges Q_i , those define an N dimensional hypersurface in the phase space known as the KAM tori. For such systems, the phase space trajectory flows are complete and they appear with a nicely foliated picture of the phase space. Different initial conditions give rise to different sets of trajectories in the phase space those are in the form of the tori. In numerical investigations, Poincare sections² (see Fig. 1) are essentially the footprints of such foliations in the phase space [2]. As the strength of the non-integrable deformation increases, most of these tori get destroyed and one essentially runs away from the foliation picture. This results into a chaotic motion and Poincare sections lose its structure, eventually becoming like a random distribution of points in the phase space.

Lyapunov exponents (see Fig.2), on the other hand, are the signature trademarks of a chaotic motion. They encode the sensitivity of the phase space trajectories on the initial conditions and are defined as³ [1]-[3]

$$\lambda = \lim_{t \rightarrow \infty} \lim_{\Delta X_0 \rightarrow 0} \frac{1}{t} \log \frac{\Delta X(X_0, t)}{\Delta X(X_0, 0)}, \quad (1)$$

¹Three parameter β deformed backgrounds can also be obtained following a TsT transformation of $AdS_4 \times CP^3$ [35]. On a similar note, a three parameter dipole deformation as well as gravity duals for noncommutative ABJM were also obtained by applying TsT transformations on $AdS_4 \times CP^3$ backgrounds [35].

²It is a lower dimensional slicing hypersurface of an N dimensional foliated KAM tori.

³For a $2N$ dimensional phase space, there are in principle $2N$ Lyapunov exponents satisfying the constraint, $\sum_{i=1}^{2N} \lambda_i = 0$. In this paper, however, we compute the largest positive Lyapunov among all these possible ones.

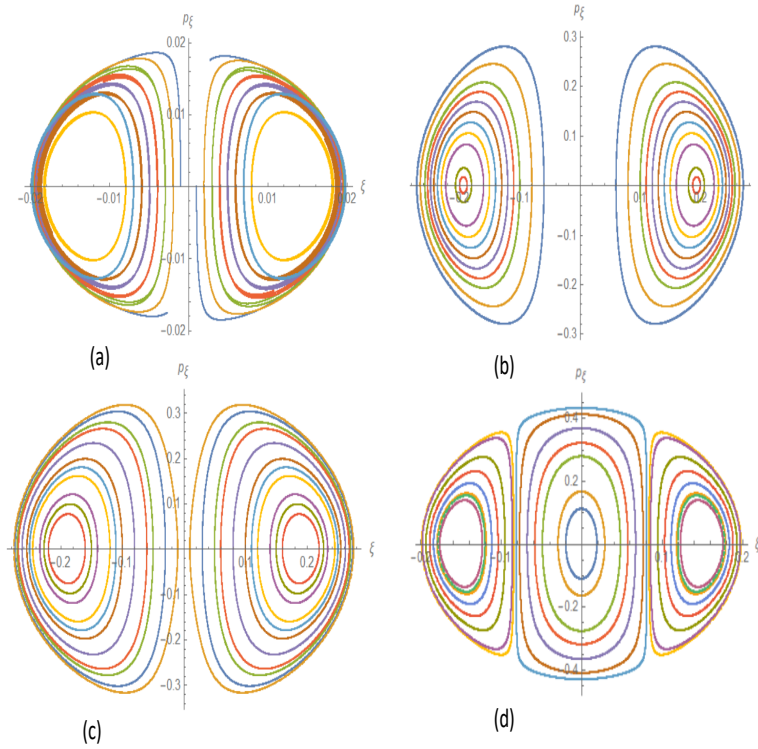


Figure 1: (a) Poincaré sections for (a) β deformed ABJM with $E = 0.01$, (b) Noncommutative ABJM with $E = 0.4$, (c) Dipole deformed ABJM with $E = 0.4$ and (d) Non-Relativistic ABJM with $E = 0.6$. Each of these Poincare sections exhibit a nice foliation for some nonzero value of the YB parameter showing an integrable structure for the associated phase space dynamics.

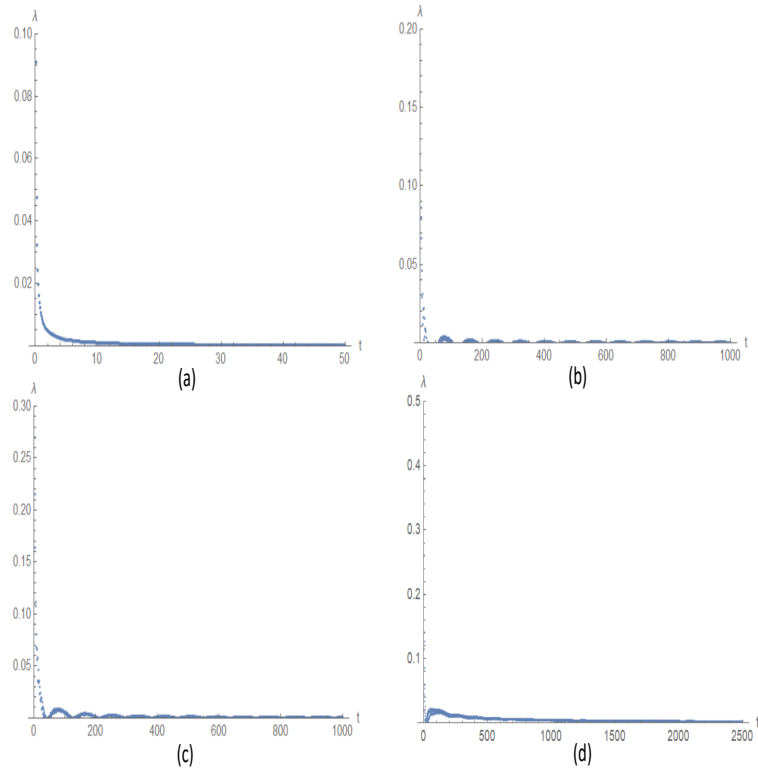


Figure 2: (a) Lyapunov exponents for (a) β deformed ABJM with $E = 0.01$, (b) Noncommutative ABJM with $E = 0.4$, (c) Dipole deformed ABJM with $E = 0.4$ and (d) Non-Relativistic ABJM with $E = 0.6$. In each of these examples, the Lyapunov approaches zero at late times which reveals an integrable structure for the phase space dynamics.

where, ΔX is the infinitesimal separation between two trajectories in the phase space. For integrable trajectories, those pertaining to a particular KAM tori, the corresponding λ approaches zero at late times. On the other hand, it exhibits a nonzero value for chaotic orbits.

To calculate the above entities in a holographic setup, one has to start with the 2D sigma model description of the form

$$S_P = -\frac{1}{2} \int d\tau d\sigma (\eta^{ab} G_{\mu\nu} + \epsilon^{ab} B_{\mu\nu}) \partial_a X^\mu \partial_b X^\nu, \quad (2)$$

where a, b are the world-sheet directions and X^μ are the target space coordinates. Here, we choose to work with the *conformal* gauge in which $\eta_{ab} = \text{diag}(-1, 1)$.

Next, we obtain the conjugate momenta as

$$p_\mu = G_{\mu\nu} \partial_\tau X^\nu + B_{\mu\nu} \partial_\sigma X^\nu, \quad (3)$$

and study the corresponding Hamilton's equations of motion (for a given string embedding) those are subjected to the Virasoro (or the Hamiltonian) constraint of the following form [1]

$$\mathcal{H} = T_{\tau\tau} = G_{\mu\nu} (\partial_\tau X^\mu \partial_\tau X^\nu + \partial_\sigma X^\mu \partial_\sigma X^\nu) \approx 0. \quad (4)$$

The above constraint (4) is always satisfied during the time evolution of the system. The initial data, that satisfy (4), are used to find solutions to the Hamilton's equations of motion corresponding to different backgrounds those are listed above. These solutions are what we call the "phase space data" those are finally used to explore the chaos indicators mentioned above.

3 Numerics and results

The purpose of this part of the analysis is to elaborate the key numerical steps those are in accordance to the algorithm that is described above. Below, we describe them in detail taking individual examples of the deformed ABJM model.

3.1 β deformed ABJM

The YB deformed background dual to β deformed ABJM is obtained by deforming the CP^3 subspace using abelian r -matrices [29] which results in the following line element

$$\begin{aligned} ds_{R \times CP^3}^2 = & -\frac{1}{4} dt^2 + d\xi^2 + \frac{1}{4} \cos^2 \xi (d\theta_1^2 + \mathcal{M} \sin^2 \theta_1 d\varphi_1^2) + \frac{1}{4} \sin^2 \xi (d\theta_2^2 + \mathcal{M} \sin^2 \theta_2 d\varphi_2^2) + \\ & \mathcal{M} \cos^2 \xi \sin^2 \xi \left(d\psi + \frac{1}{2} \cos \theta_1 d\varphi_1 - \frac{1}{2} \cos \theta_2 d\varphi_2 \right)^2 + \\ & \mathcal{M} \sin^4 \xi \cos^4 \xi \sin^2 \theta_1 \sin^2 \theta_2 (\hat{\gamma}_1 d\varphi_1 + \hat{\gamma}_2 d\varphi_2 + \hat{\gamma}_3 d\psi)^2, \end{aligned} \quad (5)$$

where we switch off the rest of the coordinates of AdS_4 .

The corresponding NS-NS two form is given by

$$\begin{aligned} B = & -\mathcal{M} \sin^2 \xi \cos^2 \xi \left[\frac{1}{2} (2\hat{\gamma}_2 + \hat{\gamma}_3 \cos \theta_2) \cos^2 \xi \sin^2 \theta_1 d\psi \wedge d\varphi_1 + \right. \\ & \frac{1}{2} (-2\hat{\gamma}_1 + \hat{\gamma}_3 \cos \theta_1) \sin^2 \xi \sin^2 \theta_2 d\psi \wedge d\varphi_2 + \frac{1}{4} \left(\hat{\gamma}_3 \sin^2 \theta_1 \sin^2 \theta_2 + \right. \\ & \left. \left. (2\hat{\gamma}_2 + \hat{\gamma}_3 \cos \theta_2) \cos^2 \xi \sin^2 \theta_1 \cos \theta_2 + (-2\hat{\gamma}_1 + \hat{\gamma}_3 \cos \theta_1) \sin^2 \xi \sin^2 \theta_2 \cos \theta_1 \right) d\varphi_1 \wedge d\varphi_2 \right], \end{aligned} \quad (6)$$

where we identify the function as

$$\mathcal{M}^{-1} = 1 + \sin^2 \xi \cos^2 \xi \left(\hat{\gamma}_3^2 \sin^2 \theta_1 \sin^2 \theta_2 + (2\hat{\gamma}_2 + \hat{\gamma}_3 \cos \theta_2)^2 \cos^2 \xi \sin^2 \theta_1 + (-2\hat{\gamma}_1 + \hat{\gamma}_3 \cos \theta_1)^2 \sin^2 \xi \sin^2 \theta_2 \right). \quad (7)$$

The winding string ansatz that we choose to work with is given by the following ansatz

$$\begin{aligned} t &= t(\tau) ; \theta_1 = \theta_1(\tau) ; \theta_2 = \theta_2(\tau) ; \xi = \xi(\tau) ; \phi_1 = \alpha_1 \tau + \alpha_2 \sigma, \\ \phi_2 &= \alpha_3 \tau + \alpha_4 \sigma ; \psi = \alpha_5 \tau + \alpha_6 \sigma, \end{aligned} \quad (8)$$

which results in a following set of Hamilton's equations of motion

$$\dot{\theta}_1 = 4p_{\theta_1} \sec^2 \xi, \quad (9)$$

$$\dot{\xi} = p_\xi, \quad (10)$$

$$p_{\dot{\theta}_1} = \frac{\cos^2 \xi \sin \theta_1 (-4 \cos \theta_1 \cos^2 \xi + 4 \sin^2 \xi + (2\hat{\gamma}_2 + \hat{\gamma}_3)^2 \cos^4 (\theta_1/2) \sin^4 (2\xi))}{16(1 + (2\hat{\gamma}_2 + \hat{\gamma}_3)^2 \cos^4 \xi \sin^2 \theta_1 \sin^2 \xi)^2}, \quad (11)$$

$$\dot{p}_\xi = \frac{\mathcal{N}_1}{(128(1 + (2\hat{\gamma}_2 + \hat{\gamma}_3)^2 \cos^4 \xi \sin^2 \theta_1 \sin^2 \xi)^2)}, \quad (12)$$

where

$$\begin{aligned} \mathcal{N}_1 &= 16(2\hat{\gamma}_2 + \hat{\gamma}_3)^2 \cos^5 \xi (-1 + 3 \cos(2\xi)) \sin^2 \theta_1 \sin^3 \xi + 32(2\hat{\gamma}_2 + \hat{\gamma}_3)^2 \cos \theta_1 \cos^5 \xi (-1 + \\ &3 \cos(2\xi)) \sin^2 \theta_1 \sin^3 \xi + (2\hat{\gamma}_2 + \hat{\gamma}_3)^2 \cos^5 \xi (-6 + 2 \cos(2\theta_1) + \cos(2\theta_1 - 2\xi) + \\ &2 \cos(2\xi) + \cos(2\theta_1 + 2\xi)) \sin^2 \theta_1 (5 \sin \xi - 3 \sin(3\xi)) - 8(1 + (2\hat{\gamma}_2 + \hat{\gamma}_3)^2 \cos^4 \xi \times \\ &\sin^2 \theta_1 \sin^2 \xi) \sin(4\xi) - 16 \cos \theta_1 (1 + (2\hat{\gamma}_2 + \hat{\gamma}_3)^2 \cos^4 \xi \sin^2 \theta_1 \sin^2 \xi) \sin(4\xi) \\ &+ 4(1 + (2\hat{\gamma}_2 + \hat{\gamma}_3)^2 \cos^4 \xi \sin^2 \theta_1 \sin^2 \xi) (4 \sin^2 \theta_1 \sin(2\xi) - 2 \cos^2 \theta_1 \sin(4\xi)) \\ &- 512p_{\theta_1}^2 \sec^2 \xi (1 + (2\hat{\gamma}_2 + \hat{\gamma}_3)^2 \cos^4 \xi \sin^2 \theta_1 \sin^2 \xi)^2 \tan \xi. \end{aligned} \quad (13)$$

In order to obtain the corresponding Poincare section (Fig.1(a)), we solve the Hamiltonian dynamics (9)-(12), subjected to the constraint (4). We set the energy ($E = E_0 = 0.01$) of the string at some particular value and choose the initial conditions as, $\theta_1(0) = 0$ and $p_\xi(0) = 0$. Given this initial set of data, we generate a random data set for an interval, $\xi(0) \in [0, 1]$ which fixes the corresponding $p_{\theta_1}(0)$ in accordance to that of the constraint (4).

With the help of this initial data set, we carry out a numerical simulation of the Hamilton's equations of motion (9)-(12), where we set the winding modes

$$\alpha_2 = \alpha_4 = \alpha_6 = 1 ; \alpha_1 = \alpha_3 = \alpha_5 = 0, \quad (14)$$

together with the YB deformation parameters as

$$\hat{\gamma}_2 = \hat{\gamma}_3 = 0.01, \quad (15)$$

where the other deformation parameter $\hat{\gamma}_1$ will disappear from the numerical simulation since we switch off the $\theta_2 = p_{\theta_2} = 0$ variables in the phase space. This is also visible from the equations of motion (9)-(12), which do not depend on the choice of $\hat{\gamma}_1$.

We plot all these points on the $\{\xi, p_\xi\}$ plane every time the trajectories pass through $\theta_1 = 0$ hyper-plane. For the present example, the phase under consideration is four dimensional, namely it is characterized by the axes $\{\theta_1, p_{\theta_1}, \xi, p_\xi\}$. Poincare sections in this case show regular patches indicating a foliation in the phase space (Fig.1(a)).

In order to calculate the Lyapunov exponent, we choose to work with the initial conditions, $E = E_0 = 0.01$ together with $\{\theta_1(0) = 0, \xi(0) = 0.008, p_{\theta_1}(0) = 0.009, p_\xi(0) = 0\}$ those are consistent with (4). With this initial set of data, we study the dynamical evolution of two nearby orbits in the phase space those have an initial separation $\Delta X_0 = 10^{-7}$. In the process, we generate a zero Lyapunov (Fig.2(a)) exhibiting a non-chaotic dynamics for the phase space.

3.2 Noncommutative ABJM

Noncommutative ABJM corresponds to a gravity dual that is obtained by applying YB deformation to its AdS_4 subspace. The corresponding abelian r -matrix is constructed using the momenta operators along AdS_4 . The resulting line element is given by [30]

$$\begin{aligned}
 ds^2 &= \frac{1}{4} \left(r^2 (-dt^2 + \mathcal{M} (dx_1^2 + dx_2^2)) + \frac{dr^2}{r^2} \right) + ds_{CP^3}^2, \\
 ds_{CP^3}^2 &= d\xi^2 + \frac{1}{4} \cos^2 \xi (d\theta_1^2 + \sin^2 \theta_1 d\phi_1^2) + \frac{1}{4} \sin^2 \xi (d\theta_2^2 + \sin^2 \theta_2 d\phi_2^2) + \\
 &\quad \left(\frac{1}{2} \cos \theta_1 d\phi_1 - \frac{1}{2} \cos \theta_2 d\phi_2 + d\psi \right)^2 \sin^2 \xi \cos^2 \xi,
 \end{aligned} \tag{16}$$

which is accompanied by a NS-NS two form

$$B = \frac{\mu \mathcal{M} r^4}{4} dx^1 \wedge dx^2, \quad \mathcal{M}^{-1} = 1 + \frac{\mu^2 r^4}{4}, \tag{17}$$

where t, x_1, x_2 and r are the coordinates of AdS_4 background. On the other hand, μ is the YB deformation parameter. Furthermore, here we set $r = 1$ for the rest of the analysis.

Next, we consider the winding string ansatz of the following form

$$\begin{aligned}
 t &= t(\tau), \quad \theta_1 = \theta_1(\tau), \quad \theta_2 = \theta_2(\tau), \quad \xi = \xi(\tau), \quad \phi_1 = \alpha_1 \tau + \alpha_2 \sigma, \quad \phi_2 = \alpha_3 \tau + \alpha_4 \sigma, \\
 \psi &= \alpha_5 \tau + \alpha_6 \sigma, \quad x_1 = \alpha_7 \tau + \alpha_8 \sigma, \quad x_2 = \alpha_9 \tau + \alpha_{10} \sigma.
 \end{aligned} \tag{18}$$

The resulting Hamilton's equations of motion are obtained as

$$\dot{\theta}_1 = 4p_{\theta_1} \sec^2 \xi, \tag{19}$$

$$\dot{\xi} = p_\xi, \tag{20}$$

$$p_{\theta_1} = \frac{1}{2} \cos^2 \xi \sin \theta_1 (-\cos \theta_1 \cos^2 \xi + \sin^2 \xi), \tag{21}$$

$$p_\xi = \frac{1}{2} \left(\cos \xi \sin^2 \theta_1 \sin \xi - \cos^4(\theta_1/2) \sin(4\xi) - 8p_{\theta_1}^2 \sec^2 \xi \tan \xi \right), \tag{22}$$

where we set, $\theta_2 = p_{\theta_2} = 0$ throughout rest of the analysis.

For numerical simulation, we set the parameters as

$$\alpha_2 = \alpha_4 = \alpha_6 = \alpha_8 = \alpha_{10} = \alpha_1 = \alpha_3 = \alpha_5 = 1 ; \alpha_7 = \alpha_9 = 0, \tag{23}$$

together with the YB deformation parameter as, $\mu = 0.01$.

In order to obtain the corresponding Poincare section (Fig.1(b)), we set the energy of the string at $E = E_0 = 0.4$, together with the initial conditions as $\theta_1(0) = 0$ and $p_\xi(0) = 0$. Like before, we generate a random data set by choosing $\xi(0) \in [0, 1]$ which fixes the initial momenta $p_{\theta_1}(0)$ following the Hamiltonian constraint (4). The $\{\xi, p_\xi\}$ cross-section is obtained by collecting the data every time the trajectory passes through the $\theta_1 = 0$ plane.

The Lyapunov (Fig.2(b)) is obtained following a similar methodology as described above. Here we set the initial conditions as $\{\theta_1(0) = 0, \xi(0) = 0.11, p_{\theta_1}(0) = 0.17, p_\xi(0) = 0\}$ together with $\Delta X_0 = 10^{-7}$. The energy of these orbits are fixed at $E = E_0 = 0.4$ such that when put together they satisfy the Hamiltonian constraint (4). In the process, we finally generate a zero Lyapunov exhibiting a non-chaotic motion.

3.3 Dipole deformed ABJM

Gravity dual of dipole deformed ABJM is obtained by considering a three parameter YB deformation of $AdS_4 \times CP^3$. The associated r -matrix is constructed combining the generators of both the AdS_4 and CP^3 subspaces. The corresponding line element is given by [30]

$$\begin{aligned}
ds^2 = & \frac{1}{4} \left(r^2 (-dx_0^2 + dx_1^2) + \frac{r^2}{1+f_3^2} dx_2^2 + \frac{dr^2}{r^2} \right) + d\xi^2 + \\
& \frac{1}{4} \cos^2 \xi (d\theta_1^2 + \sin^2 \theta_1 d\varphi_1^2) + \frac{1}{4} \sin^2 \xi (d\theta_2^2 + \sin^2 \theta_2 d\varphi_2^2) \\
& + \frac{1}{1+f_3^2} \left(\frac{1}{2} \cos \theta_1 d\varphi_1 - \frac{1}{2} \cos \theta_2 d\varphi_2 + d\psi \right)^2 \sin^2 \xi \cos^2 \xi,
\end{aligned} \tag{24}$$

together with the NS-NS fluxes

$$B = -\frac{1}{4} \left(\frac{f_3}{1+f_3^2} \right) r dx_2 \wedge \left(\frac{1}{2} \cos \theta_1 d\varphi_1 - \frac{1}{2} \cos \theta_2 d\varphi_2 + d\psi \right) \sin \xi \cos \xi, \tag{25}$$

where we identify

$$f_3 = \frac{\mu r}{2} \sin(2\xi), \tag{26}$$

and set two of the deformation parameters as $\mu_1 = \mu_2 = 0$ while the third one as $\mu_3 = \mu$. Here, r , x_0 , x_1 and x_2 are the coordinates of AdS_4 background. On the other hand ξ , θ_1 , θ_2 , ϕ_1 , ϕ_2 and ψ are the coordinates of internal CP^3 manifold. In our analysis, we choose the AdS_4 coordinates as $x_0 = t$, $x_1 = \text{constant}$ and $r = 1$.

Next, we consider the winding string ansatz of the following form

$$\begin{aligned}
t = t(\tau), \quad \theta_1 = \theta_1(\tau), \quad \theta_2 = \theta_2(\tau), \quad \xi = \xi(\tau), \quad \phi_1 = \alpha_1 \tau + \alpha_2 \sigma, \quad \phi_2 = \beta_1 \tau + \beta_2 \sigma, \\
\psi = \gamma_1 \tau + \gamma_2 \sigma, \quad x_2 = \eta_1 \tau + \eta_2 \sigma.
\end{aligned} \tag{27}$$

Next, we note down the corresponding Hamilton's equations of motion⁴

$$\dot{\theta}_1 = 4p_{\theta_1} \sec^2 \xi, \tag{28}$$

$$\dot{\xi} = p_\xi, \tag{29}$$

$$p_{\dot{\theta}_1} = \frac{\cos^4 \xi (-2 - \mu^2 + \mu^2 \cos(2\xi)) \sin(2\theta_1) + \sin \theta_1 \sin^2(2\xi)}{8 + 2\mu^2 \sin^2(2\xi)}, \tag{30}$$

$$\dot{p}_\xi = \frac{\mathcal{N}_2}{8(4 + \mu^2 \sin^2(2\xi))^2}, \tag{31}$$

where we denote

$$\begin{aligned}
\mathcal{N}_2 = & \left(-32(3 - 2\mu^2 + 4 \cos \theta_1 + \cos(2\theta_1)) \cos(2\xi) - 8(8 + \mu^2 - \mu^2 \cos(4\xi))^2 p_{\theta_1}^2 \sec^4 \xi \right. \\
& \left. + (8 + \mu^2 - \mu^2 \cos(4\xi))^2 \sin^2 \theta_1 \right) \cos \xi \sin \xi.
\end{aligned} \tag{32}$$

In order to obtain the Poincare section, we set the energy as $E = E_0 = 0.4$ while the rest of the data is chosen as $\theta_1(0) = 0$ and $p_\xi(0) = 0$. Given this initial data, we generate a random data set for $p_{\theta_1}(0)$ by choosing $\xi(0) \in [0, 1]$ such that the constraint (4) is satisfied.

⁴We choose, $\theta_2 = p_{\theta_2} = 0$ as before.

In order to run the simulation, we set $\alpha_2 = \beta_2 = \gamma_2 = \eta_2 = \alpha_1 = \beta_1 = \gamma_1 = \eta_1 = 1$ without any loss of generality. On the other hand, the YB parameter is set to be, $\mu = 0.1$. Like before, the Poincare section (Fig.1(c)) is obtained by plotting all the points those are on the $\{\xi, p_\xi\}$ plane which correspond to trajectories those pass through $\theta_1 = 0$ hyper-plane.

In order to calculate the Lyapunov exponent, we set the initial conditions as $\theta_1(0) = 0$, $p_\xi(0) = 0$, $\xi(0) = 0.1$ and $p_{\theta_1}(0) = 0.17$ those are compatible with the Hamiltonian constraint (4). The initial separation between the two nearby trajectories is set to be $\Delta X_0 = 10^{-7}$ as before, which eventually results in a zero value for the Lyapunov (Fig.2(c)).

3.4 Nonrelativistic ABJM

The gravity dual of nonrelativistic ABJM is obtained by constructing abelian r - matrices using Cartan generators of both AdS_4 as well as CP^3 subspaces. The corresponding line element is given by [30]

$$\begin{aligned}
ds^2 &= \frac{1}{4} \left(-2r^2 dx_+ dx_- + r^2 dx_1^2 + \frac{dr^2}{r^2} - \mathcal{M} r^2 dx_+^2 \right) + ds_{CP^3}^2, \\
ds_{CP^3}^2 &= d\xi^2 + \frac{1}{4} \cos^2 \xi (d\theta_1^2 + \sin^2 \theta_1 d\phi_1^2) + \frac{1}{4} \sin^2 \xi (d\theta_2^2 + \sin^2 \theta_2 d\phi_2^2) + \\
&\quad \left(\frac{1}{2} \cos \theta_1 d\phi_1 - \frac{1}{2} \cos \theta_2 d\phi_2 + d\psi \right)^2 \sin^2 \xi \cos^2 \xi,
\end{aligned} \tag{33}$$

where we denote the above functions as

$$\mathcal{M} = f_1^2 + f_2^2 + f_3^2, \tag{34}$$

$$f_1 = \frac{r}{2\sqrt{2}} \mu_1 \sin \theta_1 \cos \xi, \tag{35}$$

$$f_2 = \frac{r}{2\sqrt{2}} \mu_2 \sin \theta_2 \sin \xi, \tag{36}$$

$$f_3 = \frac{r}{2\sqrt{2}} (2\mu_3 - \mu_1 \cos \theta_1 + \mu_2 \cos \theta_2) \sin \xi \cos \xi. \tag{37}$$

The corresponding B-field is given by

$$\begin{aligned}
B &= -\frac{1}{\sqrt{2}} r \cos \xi (f_1 \sin \theta_1 - f_3 \cos \theta_1 \sin \xi) dx_+ \wedge d\varphi_1 \\
&\quad - \frac{1}{\sqrt{2}} r \sin \xi (f_3 \cos \theta_2 \cos \xi + f_2 \sin \theta_2) dx_+ \wedge d\varphi_2 \\
&\quad + \frac{1}{\sqrt{2}} r \sin(2\xi) f_3 dx_+ \wedge d\psi,
\end{aligned} \tag{38}$$

where the coordinates x_\pm are given by

$$x_\pm = \frac{1}{\sqrt{2}} (x^0 \pm x^2). \tag{39}$$

Here, $\mu_i (i = 1, 2, 3)$ are the YB deformation parameters of the theory. We choose the AdS_4 coordinates as, $x_0 = t$, $r = 1$ and $x_1 = \text{constant}$ throughout the rest of the analysis.

Next, we consider the winding string ansatz of the following form

$$\begin{aligned}
t &= t(\tau), \quad \theta_1 = \theta_1(\tau), \quad \theta_2 = \theta_2(\tau), \quad \xi = \xi(\tau), \quad \phi_1 = \alpha_1 \tau + \alpha_2 \sigma, \quad \phi_2 = \alpha_3 \tau + \alpha_4 \sigma, \\
\psi &= \alpha_5 \tau + \alpha_6 \sigma, \quad x_2 = \alpha_7 \tau + \alpha_8 \sigma.
\end{aligned} \tag{40}$$

Finally, using the embedding (40), the resulting Hamilton's equations are given by

$$\dot{\theta}_1 = 4p_{\theta_1} \sec^2 \xi, \quad (41)$$

$$\dot{\xi} = p_\xi, \quad (42)$$

$$p_{\dot{\theta}_1} = \frac{1}{128} \left(-80 \cos^4 \xi \sin(2\theta_1) + 10\mu_1 \cos^2 \xi \sin \theta_1 (\mu_1 \cos \theta_1 \cos^2 \xi + (\mu_2 + 2\mu_3) \sin^2 \xi) + 40 \sin \theta_1 \sin^2(2\xi) + \mathcal{N}_3 \right), \quad (43)$$

$$p_{\dot{\xi}} = \frac{1}{512} \left(-640 \cos^3 \xi \sin \xi - 1280 \cos \theta_1 \cos^3 \xi \sin \xi + 640 \cos \xi \sin^3 \xi + 1280 \cos \theta_1 \cos \xi \sin^3 \xi - 80(-2 + 2 \cos(2\theta_1) + \cos(2(\theta_1 - \xi)) + 2 \cos(2\xi) + \cos(2(\theta_1 + \xi))) \sin(2\xi) + \mathcal{N}_4 \right), \quad (44)$$

where the details of the functions \mathcal{N}_3 and \mathcal{N}_4 are given in the Appendix A.

Like before, we set $\theta_2 = p_{\theta_2} = 0$ throughout the rest of the analysis. The Poincare section (Fig.1(d)) is obtained by setting $E = E_0 = 0.6$ together with the initial conditions $\theta_1(0) = 0.1$ and $p_\xi(0) = 0$. The random data set for $p_{\theta_1}(0)$ is generated by choosing $\xi(0) \in [0, 1]$.

Finally, we choose the embedding parameters as $\alpha_2 = \alpha_4 = \alpha_6 = \alpha_8 = 2$, $\alpha_1 = \alpha_3 = \alpha_5 = \alpha_7 = 1$ together with the YB parameters $\mu_1 = \mu_2 = \mu_3 = 0.01$. The Poincare section is obtained by collecting the data set $\{\xi, p_\xi\}$ every time the orbits pass through the $\theta_1 = 0$ hyper-plane.

In order to calculate the Lyapunov exponent (Fig.2(d)), the corresponding initial conditions are set as $\{\theta_1(0) = 0.1, \xi(0) = 0.08, p_\xi(0) = 0, p_{\theta_1}(0) = 0.19\}$ such that the Hamiltonian constraint (4) is satisfied. The initial separation between the orbits is fixed $\Delta X_0 = 10^{-7}$ as before. This finally yield a zero Lyapunov, like in the previous three examples, showing a non-chaotic motion for the dynamical phase space under consideration.

4 Final remarks and future directions

We confirm the non-chaotic dynamics for a class of Yang-Baxter (YB) deformed $AdS_4 \times CP^3$ sigma models by estimating various chaos indicators of the theory. These backgrounds are dual to various deformations of the ABJM model [33] at strong coupling.

The (semi)classical strings, those probe these YB deformed backgrounds, are dual to a class of single trace operators in some sub-sector(s) of these deformed ABJM models. Our analysis, therefore points towards an underlying integrable structure associated with these deformed ABJM models. A systematic analysis of the Lax pairs would further strengthen this claim.

From the perspective of the deformed ABJMs, a similar investigation on the dilation operators should shed further light on an integrable structure associated with the dual QFT. This would be an interesting future direction to look for, which would eventually take us into a new class of gauge/string dualities those are associated with an underlying integrable structure.

Acknowledgments

J.P., H.R. and D.R. are indebted to the authorities of IIT Roorkee for their unconditional support towards researches in basic sciences. D.R. would also like to acknowledge The Royal Society, UK for financial assistance, and acknowledges the Grant (No. SRG/2020/000088) received from The Science and Engineering Research Board (SERB), India. Finally, we thank Arindam Lala for discussion.

A Details of the derivation (43)-(44)

The expression for \mathcal{N}_3 is given by

$$\mathcal{N}_3 = \frac{\mathcal{M}_1}{\mathcal{D}_1} - \frac{\mathcal{M}_2}{\sqrt{\mathcal{D}_1}} - \frac{\mathcal{M}_3}{64\mathcal{D}_1} - \frac{\mathcal{M}_4}{\sqrt{\mathcal{D}_1}} - \frac{\mathcal{M}_5}{8\sqrt{\mathcal{D}_1}}, \quad (\text{A1})$$

where,

$$\begin{aligned} \mathcal{M}_1 = & 4\mu_1 \cos^4 \xi \sin \theta_1 \left(\mu_1 \cos \theta_1 \cos^2 \xi + (\mu_2 + 2\mu_3) \sin^2 \xi \right) \left(\mu_1^2 \sin^2 \theta_1 + (\mu_2 + 2\mu_3 \right. \\ & \left. - \mu_1 \cos \theta_1)^2 \sin^2 \xi \right) \times \left\{ 64E + \cos^2 \xi \left[\mu_1(8\sqrt{2} + \mu_1) \sin^2 \theta_1 + \left(\mu_2^2 + 2(\mu_1(4\sqrt{2} - \mu_2 \right. \right. \right. \\ & \left. \left. - 2\mu_3) - 4\sqrt{2}(\mu_2 + 2\mu_3)) \cos \theta_1 + \mu_1(8\sqrt{2} + \mu_1) \cos^2 \theta_1 \right) \sin^2 \xi \right] + (-2\sqrt{2}\mu_2 \right. \\ & \left. - 4\sqrt{2}\mu_3 + \mu_2\mu_3 + \mu_3^2) \sin^2(2\xi) \right\}, \quad (\text{A2}) \end{aligned}$$

$$\begin{aligned} \mathcal{M}_2 = & \cos^2 \xi \sin \theta_1 \left(\mu_1^2 \sin^2 \theta_1 + (\mu_2 + 2\mu_3 - \mu_1 \cos \theta_1)^2 \sin^2 \xi \right) \times \left\{ 4\mu_1 + (8\sqrt{2} + \mu_1) \cos \theta_1 \right. \\ & \left. \cos^4 \xi + \left[\left(4\sqrt{2}(\mu_2 + 2\mu_3) + \mu_1(-4\sqrt{2} + \mu_2 + 2\mu_3) \right) \sin^2(2\xi) \right] \right\}, \quad (\text{A3}) \end{aligned}$$

$$\begin{aligned} \mathcal{M}_3 = & \mu_1 \csc^2 \xi \left(\mu_1 \cos^2 \xi \sin(2\theta_1) + 2(\mu_2 + 2\mu_3) \sin \theta_1 \sin^2 \xi \right) \sin^2(2\xi) \times \left(256E + 4\mu_1(8\sqrt{2} \right. \\ & \left. + \mu_1) \cos^2 \xi \sin^2 \theta_1 + (\mu_2 + 2\mu_3 - \mu_1 \cos \theta_1) \left(-8\sqrt{2} + \mu_2 + 2\mu_3 - (8\sqrt{2} + \mu_1) \cos \theta_1 \right) \right. \\ & \left. \sin^2(2\xi) \right)^2, \quad (\text{A4}) \end{aligned}$$

$$\begin{aligned} \mathcal{M}_4 = & \mu_1 \cos^2 \xi \left(\mu_1 \cos^2 \xi \sin(2\theta_1) + 2(\mu_2 + 2\mu_3) \sin \theta_1 \sin^2 \xi \right) \times \left\{ 128E + 2\mu_1 \cos^2 \xi \left[(8\sqrt{2} \right. \right. \\ & \left. \left. + \mu_1) \sin^2 \theta_1 + \mu_1 \cos^2 \theta_1 \sin^2 \xi \right] - \frac{1}{2}(8\sqrt{2} - \mu_2 - 2\mu_3)(\mu_2 + 2\mu_3) + \left(8\sqrt{2}(\mu_2 + 2\mu_3) \right. \right. \\ & \left. \left. + \mu_1(-8\sqrt{2} + 2\mu_2 + 4\mu_3) \cos \theta_1 - 8\sqrt{2}\mu_1 \cos^2 \theta_1 \right) \sin^2(2\xi) \right\}, \quad (\text{A5}) \end{aligned}$$

$$\begin{aligned} \mathcal{M}_5 = & \left(8\sqrt{2}(\mu_2 + 2\mu_3) + \mu_1(-8\sqrt{2} + 2\mu_2 + 4\mu_3) \sin \theta_1 + \mu_1(8\sqrt{2} + \mu_1) \cot^2 \xi \sin 2\theta_1 \right) \\ & \sin^2(2\xi) \times \left\{ -256E - 4\mu_1 \cos^2 \xi \left[(8\sqrt{2} + \mu_1) \sin^2 \theta_1 + \mu_1 \cos^2 \theta_1 \sin^2 \xi \right] + \left((8\sqrt{2} \right. \right. \\ & \left. \left. - \mu_2 - 2\mu_3)(\mu_2 + 2\mu_3) + 8\sqrt{2}(\mu_2 + 2\mu_3) + \mu_1(-8\sqrt{2} + 2\mu_2 + 4\mu_3) \cos \theta_1 \right. \right. \\ & \left. \left. - 8\sqrt{2}\mu_1 \cos^2 \theta_1 \right) \sin^2(2\xi) \right\}, \quad (\text{A6}) \end{aligned}$$

$$\begin{aligned} \mathcal{D}_1 = & \left\{ 16 + \cos^2 \xi \left[\mu_1^2 \sin^2 \theta_1 + \left(\mu_2^2 - 2\mu_1(\mu_2 + 2\mu_3) \cos \theta_1 + \mu_1^2 \cos^2 \theta_1 \right) \sin^2 \xi \right] + \mu_3(\mu_2 \right. \\ & \left. + \mu_3) \sin^2(2\xi) \right\}^2. \quad (\text{A7}) \end{aligned}$$

The expression for \mathcal{N}_4 is given by

$$\mathcal{N}_4 = -\frac{\mathcal{M}_6}{\mathcal{D}_2} - \frac{\mathcal{M}_7}{\mathcal{D}_3} + \frac{\mathcal{M}_8}{\mathcal{D}_1} + \frac{2\mathcal{M}_9}{\sqrt{\mathcal{D}_1}} - \frac{\mathcal{M}_{10}}{\mathcal{D}_1} + \mathcal{M}_{11} + \frac{\mathcal{M}_{12}}{\sqrt{\mathcal{D}_1}}, \quad (\text{A8})$$

where,

$$\begin{aligned} \mathcal{M}_6 = & 2(\mu_2 + 2\mu_3 - \mu_1 \cos \theta_1)^2 \csc^2 \xi \left((\mu_2 + 2\mu_3 - \mu_1 \cos \theta_1)(-8\sqrt{2} + \mu_2 \right. \\ & \left. + 2\mu_3 - (8\sqrt{2} + \mu_1) \cos \theta_1 \cos^2 \xi) + 64E \csc^2 \xi + \mu_1(8\sqrt{2} + \mu_1) \cot^2 \xi \sin^2 \theta_1 \right) \sin^3(2\xi), \end{aligned} \quad (\text{A9})$$

$$\mathcal{D}_2 = (\mu_2 + 2\mu_3 - \mu_1 \cos \theta_1)^2 \cos^2 \xi + 16 \csc^2 \xi + \mu_1^2 \cot^2 \xi \sin^2 \theta_1, \quad (\text{A10})$$

$$\begin{aligned} \mathcal{M}_7 = & 2 \cos^2 \xi \left(-16\sqrt{2}\mu_1 - 2\mu_1^2 + 2\mu_1(8\sqrt{2} + \mu_1) \cos(2\theta_1) + 4(\mu_1(4\sqrt{2} - \mu_2 - 2\mu_3) \right. \\ & - 4\sqrt{2}(\mu_2 + 2\mu_3)) \cos(\theta_1 - 2\xi) + 8\sqrt{2}\mu_1 \cos(2(\theta_1 - \xi)) + \mu_1^2 \cos(2(\theta_1 - \xi)) \\ & + 16\sqrt{2}\mu_1 \cos(2\xi) + 2\mu_1^2 \cos(2\xi) - 32\sqrt{2}\mu_2 \cos(2\xi) + 4\mu_2^2 \cos(2\xi) - 64\sqrt{2}\mu_3 \cos(2\xi) \\ & + 16\mu_2\mu_3 \cos(2\xi) + 16\mu_3^2 \cos(2\xi) + 8\sqrt{2}\mu_1 \cos(2(\theta_1 + \xi)) + \mu_1^2 \cos(2(\theta_1 + \xi)) \\ & + 16\sqrt{2}\mu_1 \cos((\theta_1 + 2\xi)) - 16\sqrt{2}\mu_2 \cos((\theta_1 + 2\xi)) - 4\mu_1\mu_2 \cos((\theta_1 + 2\xi)) \\ & \left. - 32\sqrt{2}\mu_3 \cos((\theta_1 + 2\xi)) - 8\mu_1\mu_3 \cos((\theta_1 + 2\xi)) \right) \left(\mu_1^2 \sin^2 \theta_1 + (\mu_2 + 2\mu_3 - \mu_1 \cos \theta_1)^2 \right. \\ & \left. \sin^2 \xi \right) \sin(2\xi), \end{aligned} \quad (\text{A11})$$

$$\mathcal{D}_3 = 16 + \cos^2 \xi \left(\mu_1^2 \sin^2 \theta_1 + (\mu_2 - \mu_1 \cos \theta_1)(\mu_2 + 4\mu_3 - \mu_1 \cos \theta_1) \sin^2 \xi \right) + \mu_3^2 \sin^2(2\xi), \quad (\text{A12})$$

$$\begin{aligned} \mathcal{M}_8 = & 2 \cos^2 \xi \left(-2\mu_1^2 + 2\mu_1^2 \cos(2\theta_1) - 4\mu_1(\mu_2 + 2\mu_3) \cos(\theta_1 - 2\xi) + \mu_1^2 \cos(2(\theta_1 - \xi)) \right. \\ & + 2\mu_1^2 \cos(2\xi) + 4\mu_2^2 \cos(2\xi) + 16\mu_2\mu_3 \cos(2\xi) + 16\mu_3^2 \cos(2\xi) + \mu_1^2 \cos(2(\theta_1 - \xi)) \\ & \left. - 4\mu_1\mu_2 \cos(\theta_1 + 2\xi) - 8\mu_1\mu_3 \cos(\theta_1 + 2\xi) \right) \left(\mu_1^2 \sin^2 \theta_1 + (\mu_2 + 2\mu_3 - \mu_1 \cos \theta_1)^2 \sin^2 \xi \right) \\ & (\sin(2\xi)) \times \left\{ 64E + \cos^2 \xi \left[\mu_1(8\sqrt{2} + \mu_1) \sin^2 \theta_1 + \left(\mu_2^2 + 2(\mu_1(4\sqrt{2} - \mu_2 - 2\mu_3) \right. \right. \right. \\ & \left. \left. - 4\sqrt{2}(\mu_2 + 2\mu_3)) \cos \theta_1 + \mu_1(8\sqrt{2} + \mu_1) \cos^2 \theta_1 \right) \sin^2 \xi \right] + (-2\sqrt{2}\mu_2 - 4\sqrt{2}\mu_3 + \mu_2\mu_3 \right. \\ & \left. + \mu_3^2) \sin^2(2\xi) \right\}, \end{aligned} \quad (\text{A13})$$

$$\begin{aligned}
\mathcal{M}_9 = & \left(-16\sqrt{2}\mu_1 - 2\mu_1^2 + 2\mu_1(8\sqrt{2} + \mu_1) \cos(2\theta_1) + 4(\mu_1(4\sqrt{2} - \mu_2 - 2\mu_3) - 4\sqrt{2}(\mu_2 \right. \\
& + 2\mu_3)) \cos(\theta_1 - 2\xi) + 8\sqrt{2}\mu_1 \cos(2(\theta_1 - \xi)) + \mu_1^2 \cos(2(\theta_1 - \xi)) + 16\sqrt{2}\mu_1 \cos(2\xi) \\
& + 2\mu_1^2 \cos(2\xi) - 32\sqrt{2}\mu_2 \cos(2\xi) + 4\mu_2^2 \cos(2\xi) - 64\sqrt{2}\mu_3 \cos(2\xi) + 16\mu_2\mu_3 \cos(2\xi) \\
& + 16\mu_3^2 \cos(2\xi) + 8\sqrt{2}\mu_1 \cos(2(\theta_1 + \xi)) + \mu_1^2 \cos(2(\theta_1 + \xi)) + 16\sqrt{2}\mu_1 \cos((\theta_1 + 2\xi)) \\
& - 16\sqrt{2}\mu_2 \cos((\theta_1 + 2\xi)) - 4\mu_1\mu_2 \cos((\theta_1 + 2\xi)) - 32\sqrt{2}\mu_3 \cos((\theta_1 + 2\xi)) - 8\mu_1\mu_3 \\
& \left. \cos((\theta_1 + 2\xi)) \right) \sin(2\xi) \times \left\{ 64E + \cos^2 \xi \left[\mu_1(8\sqrt{2} + \mu_1) \sin^2 \theta_1 + \left(\mu_2^2 + 2(\mu_1(4\sqrt{2} \right. \right. \right. \\
& - \mu_2 - 2\mu_3) - 4\sqrt{2}(\mu_2 + 2\mu_3)) \cos \theta_1 + \mu_1(8\sqrt{2} + \mu_1) \cos^2 \theta_1 \left. \left. \left. \right) \sin^2 \xi \right] + (-2\sqrt{2}\mu_2 \right. \\
& \left. - 4\sqrt{2}\mu_3 + \mu_2\mu_3 + \mu_3^2) \sin^2(2\xi) \right\}, \tag{A14}
\end{aligned}$$

$$\begin{aligned}
\mathcal{M}_{10} = & \left(-2\mu_1^2 + 2\mu_1^2 \cos(2\theta_1) - 4\mu_1(\mu_2 + 2\mu_3) \cos(\theta_1 - 2\xi) + \mu_1^2 \cos(2(\theta_1 - \xi)) \right. \\
& + 2\mu_1^2 \cos(2\xi) + 4\mu_2^2 \cos(2\xi) + 16\mu_2\mu_3 \cos(2\xi) + 16\mu_3^2 \cos(2\xi) + \mu_1^2 \cos(2(\theta_1 + \xi)) - 4\mu_1\mu_2 \\
& \left. \cos(\theta_1 + 2\xi) - 8\mu_1\mu_3 \cos(\theta_1 + 2\xi) \right) (\sin(2\xi)) \times \left\{ 64E + \cos^2 \xi \left[\mu_1(8\sqrt{2} + \mu_1) \sin^2 \theta_1 \right. \right. \\
& + \left(\mu_2^2 + 2(\mu_1(4\sqrt{2} - \mu_2 - 2\mu_3) - 4\sqrt{2}(\mu_2 + 2\mu_3)) \cos \theta_1 + \mu_1(8\sqrt{2} + \mu_1) \cos^2 \theta_1 \right) \\
& \left. \left. \sin^2 \xi \right] + (-2\sqrt{2}\mu_2 - 4\sqrt{2}\mu_3 + \mu_2\mu_3 + \mu_3^2) \sin^2(2\xi) \right\}^2, \tag{A15}
\end{aligned}$$

$$\begin{aligned}
\mathcal{M}_{11} = & 20 \left\{ 2(\mu_2 - \mu_1 \cos \theta_1)(\mu_2 + 4\mu_3 - \mu_1 \cos \theta_1) \cos^3 \xi \sin \xi - 2 \sin \xi \cos \xi \left(\mu_1^2 \sin^2 \theta_1 \right. \right. \\
& \left. \left. + (\mu_2 - \mu_1 \cos \theta_1)(\mu_2 + 4\mu_3 - \mu_1 \cos \theta_1) \sin^2 \xi \right) + 2\mu_3^2 \sin^2(4\xi) - 2048p_{\theta_1}^2 \sec^2 \xi \tan \xi \right\}, \tag{A16}
\end{aligned}$$

$$\begin{aligned}
\mathcal{M}_{12} = & 16 \cos \xi \sin \xi \left(\mu_1^2 \sin^2 \theta_1 + (\mu_2 + 2\mu_3 - \mu_1 \cos \theta_1)^2 \sin^2 \xi \right) \\
& \times \left\{ 64E + \cos^2 \xi \left[\mu_1(8\sqrt{2} + \mu_1) \sin^2 \theta_1 + \left(\mu_2^2 + 2(\mu_1(4\sqrt{2} - \mu_2 - 2\mu_3) \right. \right. \right. \\
& - 4\sqrt{2}(\mu_2 + 2\mu_3)) \cos \theta_1 + \mu_1(8\sqrt{2} + \mu_1) \cos^2 \theta_1 \left. \left. \left. \right) \sin^2 \xi \right] + (-2\sqrt{2}\mu_2 \right. \\
& \left. - 4\sqrt{2}\mu_3 + \mu_2\mu_3 + \mu_3^2) \sin^2(2\xi) \right\}. \tag{A17}
\end{aligned}$$

References

- [1] L. A. Pando Zayas and C. A. Terrero-Escalante, “Chaos in the Gauge / Gravity Correspondence,” JHEP 1009, 094 (2010) doi:10.1007/JHEP09(2010)094 [arXiv:1007.0277 [hep-th]].
- [2] P. Basu, D. Das and A. Ghosh, “Integrability Lost,” Phys. Lett. B 699, 388 (2011) doi:10.1016/j.physletb.2011.04.027 [arXiv:1103.4101 [hep-th]].

- [3] P. Basu and L. A. Pando Zayas, “Chaos rules out integrability of strings on $AdS_5 \times T^{1,1}$ ” Phys. Lett. B 700, 243 (2011) doi:10.1016/j.physletb.2011.04.063 [arXiv:1103.4107 [hep-th]].
- [4] P. Basu and L. A. Pando Zayas, “Analytic Non-integrability in String Theory,” Phys. Rev. D **84** (2011), 046006 doi:10.1103/PhysRevD.84.046006 [arXiv:1105.2540 [hep-th]].
- [5] P. Basu, D. Das, A. Ghosh and L. A. Pando Zayas, “Chaos around Holographic Regge Trajectories,” JHEP 1205, 077 (2012) doi:10.1007/JHEP05(2012)077 [arXiv:1201.5634 [hep-th]].
- [6] L. A. Pando Zayas and D. Reichmann, “A String Theory Explanation for Quantum Chaos in the Hadronic Spectrum,” JHEP 1304, 083 (2013) doi:10.1007/JHEP04(2013)083 [arXiv:1209.5902 [hep-th]].
- [7] P. Basu and A. Ghosh, “Confining Backgrounds and Quantum Chaos in Holography,” Phys. Lett. B 729, 50 (2014) doi:10.1016/j.physletb.2013.12.052 [arXiv:1304.6348[hep-th]].
- [8] P. Basu, P. Chaturvedi and P. Samantray, “Chaotic dynamics of strings in charged black hole backgrounds,” Phys. Rev. D **95**, no.6, 066014 (2017) doi:10.1103/PhysRevD.95.066014 [arXiv:1607.04466 [hep-th]].
- [9] K. L. Panigrahi and M. Samal, “Chaos in classical string dynamics in $\hat{\gamma}$ deformed $AdS_5 \times T^{1,1}$,” Phys. Lett. B **761**, 475-481 (2016) doi:10.1016/j.physletb.2016.08.021 [arXiv:1605.05638 [hep-th]].
- [10] D. Giataganas, L. A. Pando Zayas and K. Zoubos, “On Marginal Deformations and Non-Integrability,” JHEP 1401, 129 (2014) doi:10.1007/JHEP01(2014)129 [arXiv:1311.3241 [hep-th]].
- [11] T. Ishii, S. Kushiro and K. Yoshida, “Chaotic string dynamics in deformed $T^{1,1}$,” JHEP **05**, 158 (2021) doi:10.1007/JHEP05(2021)158 [arXiv:2103.12416 [hep-th]].
- [12] D. Roychowdhury, “Analytic integrability for strings on η and λ deformed backgrounds,” JHEP **10** (2017), 056 doi:10.1007/JHEP10(2017)056 [arXiv:1707.07172 [hep-th]].
- [13] C. Núñez, J. M. Penín, D. Roychowdhury and J. Van Gersel, “The non-Integrability of Strings in Massive Type IIA and their Holographic duals,” JHEP **06** (2018), 078 doi:10.1007/JHEP06(2018)078 [arXiv:1802.04269 [hep-th]].
- [14] C. Núñez, D. Roychowdhury and D. C. Thompson, “Integrability and non-integrability in $\mathcal{N} = 2$ SCFTs and their holographic backgrounds,” JHEP **07** (2018), 044 doi:10.1007/JHEP07(2018)044 [arXiv:1804.08621 [hep-th]].
- [15] J. M. Maldacena, “The Large N limit of superconformal field theories and supergravity,” Adv. Theor. Math. Phys. **2** (1998), 231-252 doi:10.1023/A:1026654312961 [arXiv:hep-th/9711200 [hep-th]].
- [16] E. Witten, “Anti-de Sitter space and holography,” Adv. Theor. Math. Phys. **2** (1998), 253-291 doi:10.4310/ATMP.1998.v2.n2.a2 [arXiv:hep-th/9802150 [hep-th]].
- [17] C. Klimcik, “Yang-Baxter sigma models and dS/AdS T duality,” JHEP **12**, 051 (2002) doi:10.1088/1126-6708/2002/12/051 [arXiv:hep-th/0210095 [hep-th]].
- [18] C. Klimcik, “On integrability of the Yang-Baxter sigma-model,” J. Math. Phys. **50**, 043508 (2009) doi:10.1063/1.3116242 [arXiv:0802.3518 [hep-th]].

- [19] F. Delduc, M. Magro and B. Vicedo, “On classical q -deformations of integrable sigma-models,” JHEP **11**, 192 (2013) doi:10.1007/JHEP11(2013)192 [arXiv:1308.3581 [hep-th]].
- [20] F. Delduc, M. Magro and B. Vicedo, “An integrable deformation of the $AdS_5 \times S^5$ superstring action,” Phys. Rev. Lett. **112**, no.5, 051601 (2014) doi:10.1103/PhysRevLett.112.051601 [arXiv:1309.5850 [hep-th]].
- [21] F. Delduc, M. Magro and B. Vicedo, “Derivation of the action and symmetries of the q -deformed $AdS_5 \times S^5$ superstring,” JHEP **10**, 132 (2014) doi:10.1007/JHEP10(2014)132 [arXiv:1406.6286 [hep-th]].
- [22] G. Arutyunov, R. Borsato and S. Frolov, “S-matrix for strings on η -deformed $AdS_5 \times S^5$,” JHEP **04**, 002 (2014) doi:10.1007/JHEP04(2014)002 [arXiv:1312.3542 [hep-th]].
- [23] G. Arutyunov, S. Frolov, B. Hoare, R. Roiban and A. A. Tseytlin, “Scale invariance of the η -deformed $AdS_5 \times S^5$ superstring, T-duality and modified type II equations,” Nucl. Phys. B **903**, 262-303 (2016) doi:10.1016/j.nuclphysb.2015.12.012 [arXiv:1511.05795 [hep-th]].
- [24] B. Hoare and F. K. Seibold, “Supergravity backgrounds of the η -deformed $AdS_2 \times S^2 \times T^6$ and $AdS_5 \times S^5$ superstrings,” JHEP **01**, 125 (2019) doi:10.1007/JHEP01(2019)125 [arXiv:1811.07841 [hep-th]].
- [25] I. Kawaguchi, T. Matsumoto and K. Yoshida, “Jordanian deformations of the $AdS_5 \times S^5$ superstring,” JHEP **04**, 153 (2014) doi:10.1007/JHEP04(2014)153 [arXiv:1401.4855 [hep-th]].
- [26] D. Orlando, S. Reffert, J. i. Sakamoto and K. Yoshida, “Generalized type IIB supergravity equations and non-Abelian classical r-matrices,” J. Phys. A **49**, no.44, 445403 (2016) doi:10.1088/1751-8113/49/44/445403 [arXiv:1607.00795 [hep-th]].
- [27] T. Matsumoto and K. Yoshida, “Lunin-Maldacena backgrounds from the classical Yang-Baxter equation - towards the gravity/CYBE correspondence,” JHEP **06**, 135 (2014) doi:10.1007/JHEP06(2014)135 [arXiv:1404.1838 [hep-th]].
- [28] T. Matsumoto and K. Yoshida, “Schrödinger geometries arising from Yang-Baxter deformations,” JHEP **04**, 180 (2015) doi:10.1007/JHEP04(2015)180 [arXiv:1502.00740 [hep-th]].
- [29] R. Negrón and V. O. Rivelles, “Yang-Baxter deformations of the $AdS_4 \times \mathbb{CP}^3$ superstring sigma model,” JHEP **11**, 043 (2018) doi:10.1007/JHEP11(2018)043 [arXiv:1809.01174 [hep-th]].
- [30] L. Rado, V. O. Rivelles and R. Sánchez, “String backgrounds of the Yang-Baxter deformed $AdS_4 \times \mathbb{CP}^3$ superstring,” JHEP **01**, 056 (2021) doi:10.1007/JHEP01(2021)056 [arXiv:2009.04397 [hep-th]].
- [31] L. Rado, V. O. Rivelles and R. Sánchez, “Bosonic η -deformations of non-integrable backgrounds,” JHEP **03**, 094 (2022) doi:10.1007/JHEP03(2022)094 [arXiv:2111.13169 [hep-th]].
- [32] L. Rado, V. O. Rivelles and R. Sánchez, “Bosonic η -deformed $AdS_4 \times \mathbb{CP}^3$ Background,” JHEP **10**, 115 (2021) doi:10.1007/JHEP10(2021)115 [arXiv:2105.07545 [hep-th]].
- [33] O. Aharony, O. Bergman, D. L. Jafferis and J. Maldacena, “N=6 superconformal Chern-Simons-matter theories, M2-branes and their gravity duals,” JHEP **10**, 091 (2008) doi:10.1088/1126-6708/2008/10/091 [arXiv:0806.1218 [hep-th]].

- [34] G. Arutyunov and S. Frolov, “Superstrings on $AdS(4) \times CP^{*3}$ as a Coset Sigma-model,” *JHEP* **09**, 129 (2008) doi:10.1088/1126-6708/2008/09/129 [arXiv:0806.4940 [hep-th]].
- [35] E. Imeroni, “On deformed gauge theories and their string/M-theory duals,” *JHEP* **10**, 026 (2008) doi:10.1088/1126-6708/2008/10/026 [arXiv:0808.1271 [hep-th]].